

Direct observation and control of magnetic monopole defects in an artificial spin-ice material

This article has been downloaded from IOPscience. Please scroll down to see the full text article.

2011 New J. Phys. 13 063032

(<http://iopscience.iop.org/1367-2630/13/6/063032>)

View [the table of contents for this issue](#), or go to the [journal homepage](#) for more

Download details:

IP Address: 131.251.133.28

The article was downloaded on 11/04/2012 at 09:42

Please note that [terms and conditions apply](#).

Direct observation and control of magnetic monopole defects in an artificial spin-ice material

S Ladak, D E Read, W R Branford¹ and L F Cohen

Department of Physics, Blackett Laboratory, Imperial College,
Prince Consort Road, South Kensington, London SW7 2AZ, UK
E-mail: w.branford@imperial.ac.uk

New Journal of Physics **13** (2011) 063032 (11pp)

Received 10 January 2011

Published 17 June 2011

Online at <http://www.njp.org/>

doi:10.1088/1367-2630/13/6/063032

Abstract. Magnetic monopoles have stimulated a great amount of theoretical and experimental interest since their prediction by Dirac in 1931. To date, their presence has evaded detection in high energy experiments despite intensive efforts. Recently, entities that mimic magnetic monopoles have been observed in bulk and planar frustrated materials known as spin-ice materials, and artificial spin-ice materials, respectively. In this paper we discuss the formation of these so-called monopole defects within a cobalt honeycomb artificial spin-ice lattice. Experimental results and micromagnetic simulations show that monopole defects of opposite sign are created at the boundaries of the lattice, and move in opposing directions. Discrepancies between simulations and experimental results demonstrate the importance of quenched disorder. Furthermore, we show that controlled edge nucleated monopole defect formation can be realized with the use of soft magnetic injection pads, which is a very promising development for technological applications based upon magnetic charge.

¹ Author to whom any correspondence should be addressed.

Contents

1. Introduction	2
2. Method	3
3. Micromagnetic structure of ice-rule obeying states	3
4. Creation and movement of monopole defects	5
5. Simulations of monopole defect creation	6
6. Controlled monopole defect creation and the role of disorder	8
Acknowledgments	10
References	10

1. Introduction

Spin-ice materials were first discovered in 1997 and have enabled detailed studies of the physics of frustration [1]. These materials consist of moments on corner-sharing tetrahedra, each of which points along its local Ising axis along the [111] direction. The moments cannot satisfy all nearby pair-wise interactions, leading to frustration and a minimum energy configuration of the system when two spins point in and two point out of the center of the tetrahedra, a configuration known as ‘ice rules’ due to its similarities to bonding in water ice [2]. Apart from providing a clean system to study frustration, these materials have recently been shown to support exotic excitations where the magnetic properties are found to fractionalize. The emergent quasiparticles carry magnetic charge and no magnetic moment and their interactions are described by a simple magnetic Coulomb’s law, and so are considered to be magnetic monopoles [3]. There is now overwhelming evidence that these monopoles do indeed exist in spin-ice materials and their study may lead to clues about the dynamics of fundamental monopoles in the early universe, or stimulate the design of exotic magnetoelectronic devices based upon magnetic charge. Unfortunately, the study of magnetic monopoles and the string connecting them in these three-dimensional (3D) systems is not straightforward and typically requires neutron or muon experiments below 1 K [4]. Furthermore, the use of macroscopic scattering experiments means that the study of individual monopole creation events and dynamics is challenging, if not impossible. An alternative system to study frustration is artificial spin-ice [5]. Artificial spin-ice materials are 2D structures fabricated using standard sputtering and electron-beam lithography techniques. An example of such a structure that has been studied is the honeycomb lattice made of Co or NiFe [6, 7]. The bar dimensions in these structures are sufficiently small to ensure single domain behavior, but large enough to have a stable magnetic moment at room temperature. The ice rules in this system are manifest when two spins point into a vertex and one out (2-in/1-out), or one spin points into a vertex and two out (1-in/2-out). We have recently shown that through the use of a particular magnetic field history [6], 2D monopole defects can be created in artificial spin-ice honeycomb nanostructures made from cobalt and be seen to propagate with increments to the field. Unlike the equivalents in bulk spin-ice, these monopole defects are created as domain walls of magnetic charge $\pm 2q$, and flow through a charge ordered background of $\pm q$. The arrival of a $+2q$ domain wall upon a $+q$ vertex leads to $+3q$ monopole defect (where three spins point into a vertex), and the resulting structure has no net dipole moment. A similar situation is evident for $-2q$ domain walls arriving on a $-q$ vertex, creating a $-3q$ monopole defect (where three spins point out).

In this paper we examine the process by which monopole defects form in Co honeycomb structures. Using micromagnetic simulations we explore the transverse domain wall switching process that leads to the formation of monopole defects and compare these against experiments. In this system it is clear that quenched disorder plays an important role. By using information gained on the switching process, we are able to show how reproducible monopole defect capture may be realized.

2. Method

Samples were fabricated by sputtering 20 nm thick Co thin films followed by standard e-beam lithography and ion-beam milling. The growth rate was calibrated and the thickness was also confirmed by vibrating sample magnetometry of the unprocessed film. After fabrication of the honeycomb, the sample features were checked by SEM to ensure the pattern was of good quality. The individual bars on the honeycomb had dimensions of approximately $1000 \text{ nm} \times 100 \text{ nm}$. The spatial extent of the honeycomb was $100 \mu\text{m} \times 100 \mu\text{m}$, and 12 injection pads of width $8 \mu\text{m}$ were terminated on the edge of the honeycomb square (three injection pads on each side).

Magnetic force microscopy (MFM) was carried out with a Digital Instruments 3100 series model at room temperature. The system was fitted with a custom-made electromagnet, which allowed a field to be applied in the range of 100 mT in the plane of the sample. MFM tips used in this study were standard MESP tips supplied by Veeco which had a coercivity of approximately 60 mT. MFM studies were performed at remanence in order to demonstrate the creation and movement of monopole defects in the absence of a field. Further high-resolution MFM measurements were carried out on both ice-rule states and monopole defect states in order to understand the local micromagnetic structure. Micromagnetic simulations were carried out with the object orientated micro-magnetic framework (OOMMF)² [8] on a 10×10 honeycomb array. The OOMMF software solves the Landau–Lifshitz equation at each point on a rectangular mesh:

$$\frac{dM}{dt} = -\gamma(M \times H_{\text{eff}}) + \alpha \left(M \times \frac{dM}{dt} \right),$$

where $H_{\text{eff}} = -\nabla_M E$ and E is the free energy which includes terms for the Zeeman, demagnetization, exchange and the anisotropy energies. A cell size of 5 nm was used to construct the mesh, and the magnetization was allowed to relax, in the absence of an applied magnetic field in order to find a minimum energy configuration. The magnetocrystalline anisotropy of cobalt was assumed to be zero, the exchange stiffness was taken to be $1.3 \times 10^{-11} \text{ J m}^{-1}$, and the saturation magnetization of Co was assumed to be 1400 emu cm^{-3} . In order to study the switching a field of 100 mT was applied along the x - direction.

3. Micromagnetic structure of ice-rule obeying states

Before studying the detailed reversal mechanisms leading to monopole defect formation, it is important to precondition the sample, and understand the micromagnetic structure of the standard ice rules at remanence. Figure 1(a) shows an MFM image which has been obtained after saturating the sample in the negative x -direction. An ordering of alternating positive and

² The OOMMF code is available at <http://math.nist.gov/oommf>.

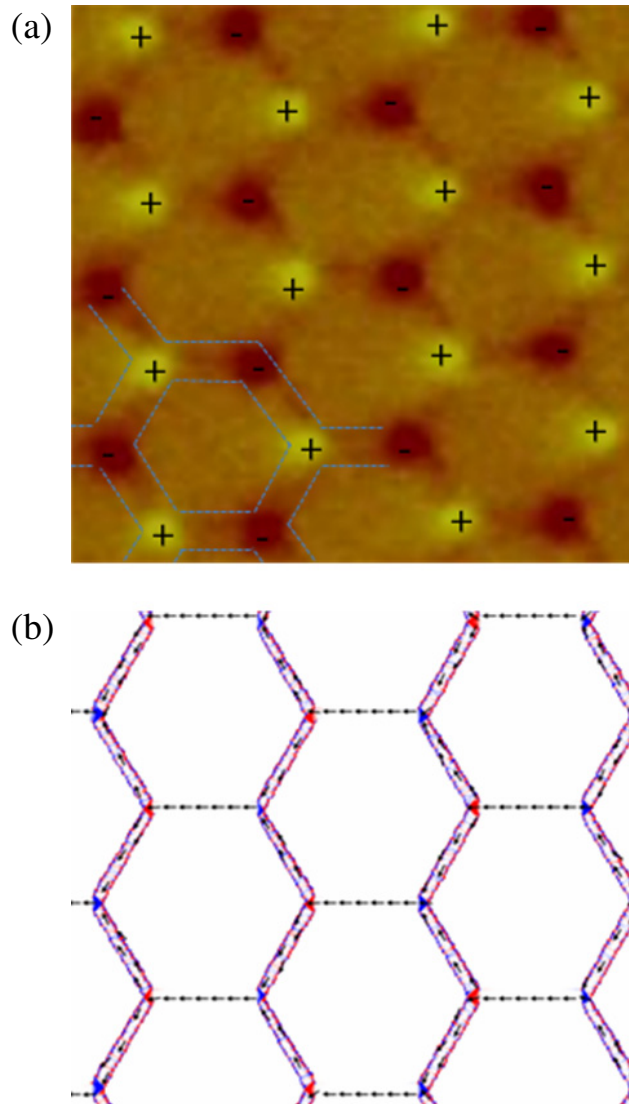


Figure 1. (a) MFM image of the honeycomb array after application of a saturating field in the negative field direction ($-x$). (b) Simulations carried out with the OOMMF package after a similar field was applied. Red and blue colour contrast corresponds to positive and negative $\text{Div}(\mathbf{M})$, respectively.

negative magnetic charge, $Q = \pm q$, is observed on vertices. The equal intensity of the spots in the image indicates that only ice-rule obeying states are observed. Micromagnetic simulations after the application of the same field are shown in figure 1(b). In this image the red and blue contrast corresponds to positive and negative magnetic charge density, $\rho_M = \nabla \cdot \mathbf{M}$, the source of which is a finite divergence of \mathbf{M} at the vertices. It is well known that MFM measures $d^2 H_z / dz^2$, which has high values in these images due to stray fields emanating from the finite magnetic charge at vertices. Hence, a qualitative comparison can be made between the contrast in the simulations and the contrast in the MFM images, as has been shown previously [9]. The application of the large negative field leads all of the individual bars to switch so that they have a component along the field direction, as shown in figure 1(b). The magnetic charge

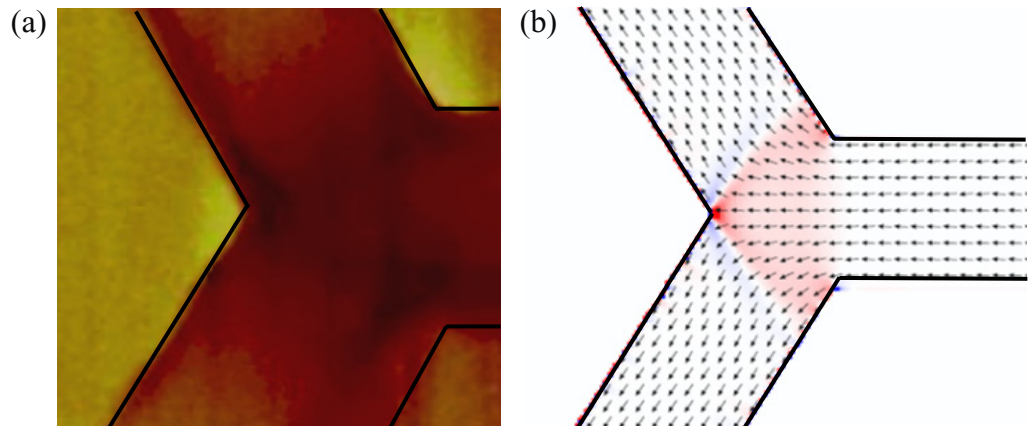


Figure 2. (a) High resolution MFM image of an ice-rule state. (b) The corresponding magnetization distribution and $\text{Div}(\mathbf{M})$ contrast determined by simulations.

density in the simulation matches that of the MFM and also indicates a long-range ordering throughout the lattice. No monopole defects are seen in this state, either in the simulations or in the MFM images. Figures 2(a) and (b) show a high-resolution image of an ice-rule state and the corresponding micromagnetic simulation, respectively. The ice-rule state consists of a state where the magnetization gradually rotates out from the horizontal bar to a 60° angle within the plane. This leads to a maximum in magnetic charge density at the three corners of the vertex and hence strong MFM contrast. There is excellent agreement between simulations and MFM contrast.

4. Creation and movement of monopole defects

Our methodology for creating monopole defects on the lattice is to saturate the sample in one direction, as described in section 3, and then drive the structure through a partial reversal process. A field of approximately 100 mT was applied along the positive x -direction. The field was then reduced and decreased to negative fields in small increments of 0.6 mT). A MFM image was taken at remanence after the application of the field. Figure 3 shows a series of MFM images taken at incrementing field values. At approximately -48.8 mT, the first monopole defects (bright features) start appearing at some of the vertices, as shown in figure 3(b). The monopole defects have a phase intensity of approximately three times that of the standard ice-rule, indicating a magnetic charge of $Q = 3q$ but no local magnetic dipole moment ($M = 0$). As the field increases (figures 3(c)–(l)), the monopole defects hop to adjacent sites, with positive monopole defects hopping to the right, and negative to the left. The conserved quantities carrying magnetic charge in this case are transverse domain walls carrying $\pm 2q$ as they hop through the charge ordered background of $\pm q$, shown in figure 1. Careful examination of figure 3 [10] shows that monopole defects are not created in a single-step process. Instead, we typically observe the switching of a single diagonal bar first, followed by the switching of the connected horizontal bar as is demonstrated schematically in figures 4(a)–(c).

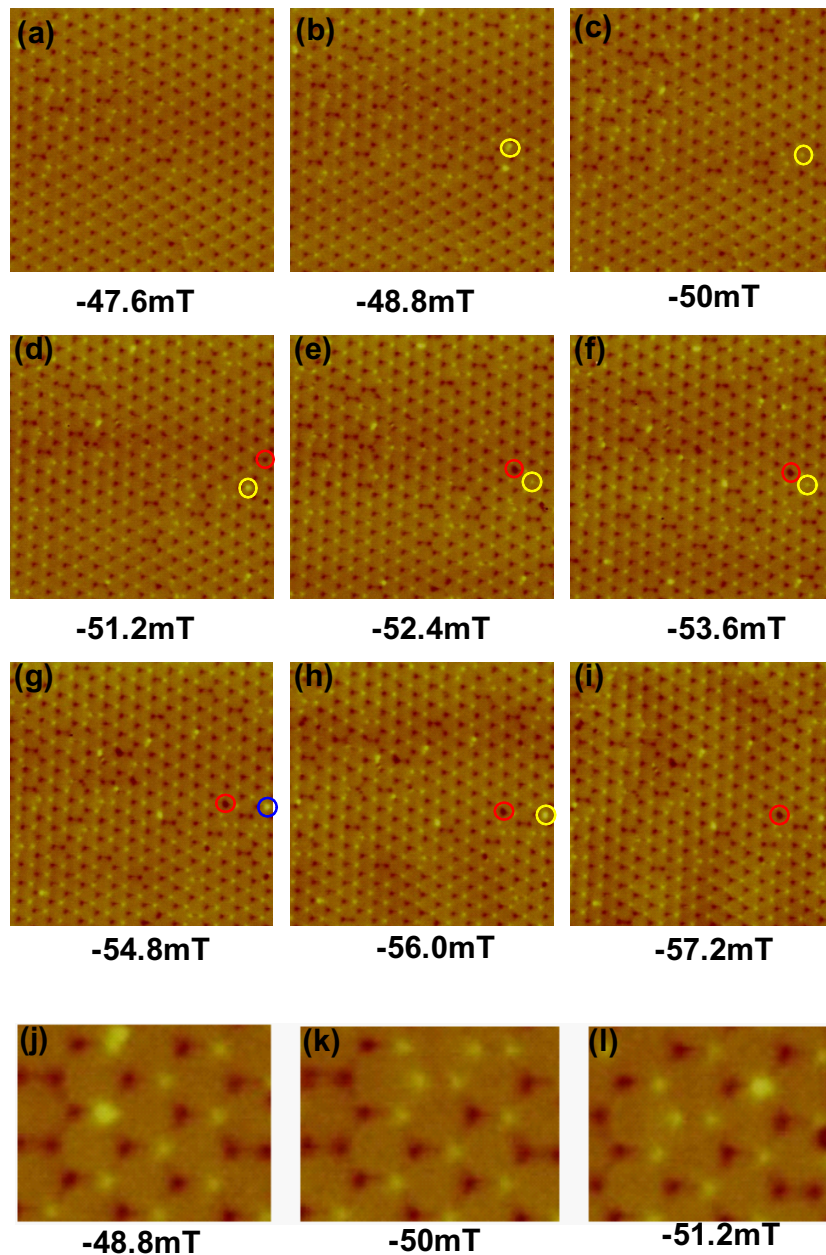


Figure 3. (a–i) The movement of magnetic monopole defects through the honeycomb lattice. Yellow and red circles highlight the movement of positive and negative monopole defects, respectively. Positive monopoles defects are seen to move to the right and negative monopole defects are seen to move to the left. (j–l) Expanded view of the two-stage process creating the (circled) monopole defect in images (a–c).

5. Simulations of monopole defect creation

The experimental data shown in section 4 indicates that the creation and movement of monopole defects is mediated through the nucleation and movement of transverse domain walls through

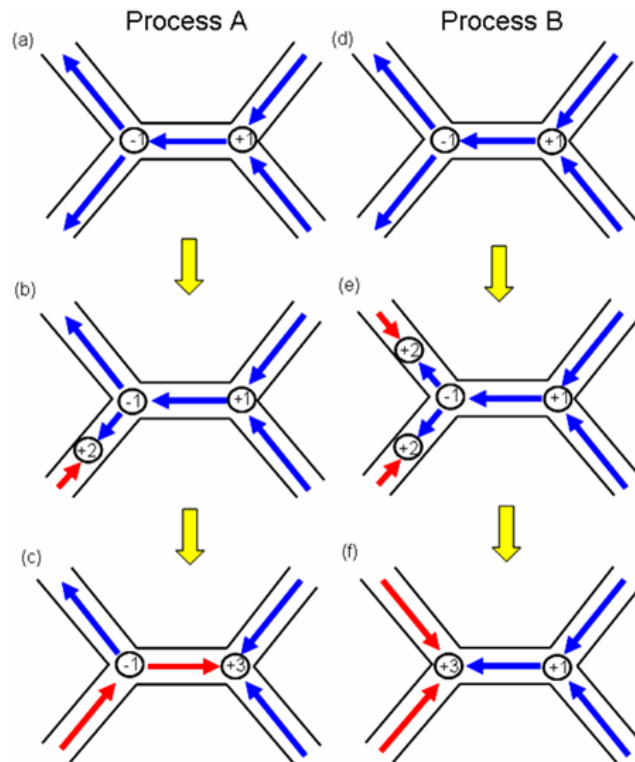


Figure 4. Two possible ways to create a monopole defect. In process A (a–c), a domain wall nucleates along a single diagonal bar, and then propagates down the attached horizontal bar, creating a $+3q$ monopole defect state. In process B, (d–f) two domain walls are created on diagonal bars and propagate up towards the vertex area, creating a $+3q$ monopole defect state.

the lattice. In order to understand initial domain wall nucleation processes in more detail, a micromagnetic simulation (see method for details) was carried out on a *perfectly ordered array*. The array was first saturated in the positive field direction, leading to each vertex in the entire array being in an ice-rule state, as shown in figure 1(b). The field was subsequently reduced to zero and increased in the negative field direction. The simulation indicates that magnetic reversal occurs first at the boundary, and figure 5 shows the nucleation and movement of domain walls at the boundary. As the field in the negative x-direction increases, the torque $-(M \times H_{\text{eff}})$ is largest upon the diagonal bars. The demagnetization energy keeps the magnetic moments pointing along the bars, but as the Zeeman energy increases the magnetization cants away from the bar direction and at a threshold field head-to-head transverse domain walls nucleate at the vertex boundary. The transverse domain walls propagate through the bars, as shown in figures 5(b) and (c), until they reach the edge of the vertex where they are pinned. A similar process occurs for creation of negative monopole defects (three out states). In this case tail-to-tail domain walls are created at the opposite boundary. Hence, in a perfectly ordered array, monopole defects of opposite sign are most prominent at opposite edges of the lattice early on in the magnetic reversal process and are created by a two-domain wall process shown schematically in figures 4(d)–(f).

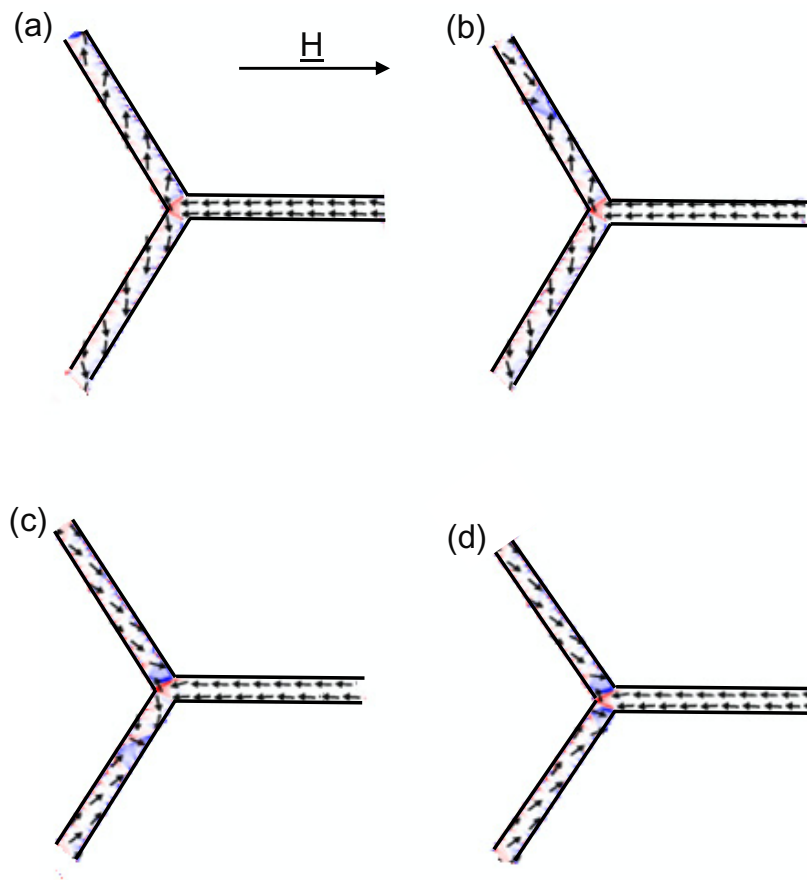


Figure 5. Micromagnetic switching, which leads to the formation of monopole defects on the boundary of the lattice. (a) 40 mT: torque on diagonal bars leads to M canting away from local easy axis. (b–d) 50–52 mT: head-to-head domain walls are created at the boundaries and propagate down the diagonal bars. They are eventually pinned at the vertex area.

6. Controlled monopole defect creation and the role of disorder

The creation and motion of domain walls within the array is well described by their magnetic coulomb interactions with the global field and local magnetic charges within the array. Thus the creation of a head to head ($+2q$) domain wall requires a $+q$ vertex to become a $-q$ vertex and the global nucleation field must be sufficient to overcome the local Coulomb attraction between the $+2q$ wall and the $-q$ vertex. If all vertices are exactly equivalent then that nucleation field will be exactly enough to overcome the Coulomb repulsion at a neighboring $+q$ vertex, creating a transient $+3q$ vertex and then driving the wall onward through the array and returning the transient $+3$ to the $+1$ state. As the nucleation field is also exactly sufficient to drive the wall away from other identical oppositely charged vertices, nucleation immediately results in long cascades to the array boundaries [11]. The formation of stable $+3q$ or $-3q$ monopole defects requires that this equivalence be broken. There are two mechanisms by which this can occur, quenched disorder or magnetic Coulomb blockade [12]. In the cobalt arrays studied here the exact magnetic charge distribution at the vertices appears very sensitive to small variations

in the material (quenched disorder), such as width, thickness and roughness, and so there is a substantial variation in nucleation and depinning field between vertices. This dramatically reduces the average cascade length and provides a mechanism to form monopole defects in a one-domain wall process (figure 4, process A).

The micromagnetic modeling shown above indicates a tendency for monopole defects to be created at the boundaries of the lattice where there is a discontinuity in the magnetostatic energy landscape. The simulations show that a monopole defect creation event is dependent upon two domain walls being situated on diagonals leading to the same vertex (process B in figure 4). In a perfectly ordered array, and in our simulations, the domain walls are created at approximately the same nucleation field as expected. In a real array, imperfections in processing can lead to a distribution in bar coercivities, which means it is likely that a domain wall will nucleate in one diagonal bar before the other, and become pinned at a vertex. The pinning potential of a single domain wall at a vertex has a narrow field window [13], and the detailed energy profile is dependent upon the chirality of the domain wall with respect to the local magnetization direction. A small field increment is likely to de-pin the domain wall from the vertex, and move it along the horizontal bar. It should be noted that arrays fabricated with magnetically soft materials, with low intrinsic magneto crystalline anisotropy such as $\text{Ni}_{81}\text{Fe}_{19}$ appear to have a much smaller distribution of bar coercivities, and in this case we do not observe the single domain wall process A, monopole defects formation occurs only via the simulated two-domain wall process [12] shown schematically in figures 4(a)–(c) and in figure 5. Disorder in our cobalt samples shows that it is possible to engineer specific vertices to support monopole defects. However, in this particular material system it is difficult to visualize how one may controllably form monopole defects at any given vertex in the array. This is an important issue if devices based on magnetic charge are to be realized. Domain wall injection via soft pads at the boundary offers a potential solution. The pads will lead to reproducible injection of a domain wall at a threshold field such that the domain-walls are created at the same time on the boundary diagonals leading to monopole defect formation. In order to investigate the use of magnetic injection pads for controlled monopole defect creation, a study was carried out whereby the sample was taken through the full hysteresis cycle several times, and an image was taken near the boundary of an array, close to injection pads, at each field point for each cycle. Figures 6(a) and (b) show images at the same field point from different hysteresis cycles. In both images, one can see a column of monopole defects (red circles) on the same lattice sites adjacent to the magnetic injection pad, whereas monopole defects found elsewhere in the lattice are unique to that particular field cycle (blue circles). Although simulations of a perfect array suggest that monopole defects are always created at the boundary, the experiments and data shown in figure 6 suggest that the role of disorder becomes important in real samples. The above experiment suggests that there are at least two factors that need to be taken into consideration when trying to control monopole defect formation on a given site. Both relate to disorder. Quenched disorder resulting from imperfections in the lithography can lead to a distribution of bar coercivities. The creation of monopole defects is caused by domain wall motion through vertices with two possible exits, and there is no systematic differentiation across the array of the possible paths. Thus, predictability in monopole defect position decreases as one gets deeper into the array. The disorder created by these two phenomena may be addressed by better control of lithography and processing, and by using small bias fields (with H_y component) to steer domain walls in the wanted direction. Ultimately, this may lead to a device where the injection and movement of magnetic charge may be controlled with a high degree of precision.

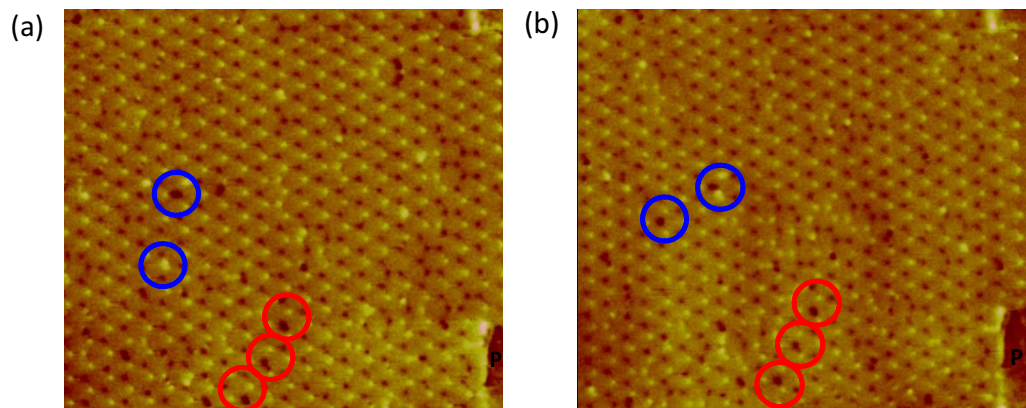


Figure 6. MFM images of honeycomb array boundary, taken at the same field point, for different field cycles. Monopole defects circled in red are reproducible on different field cycles, and those circled in blue are unique to each field cycle. The injection pad is marked 'P' and is located in the bottom right-hand side of the images.

In conclusion, the movement of monopole defects has been directly observed in an artificial spin-ice honeycomb material. The conserved magnetic charge carriers are transverse domain walls with magnetic charge $\pm 2q$, and their flow in field through a charged lattice leads to positive and negative monopole defects with magnetic charge $\pm 3q$. Simulations suggest that monopole defects are created via a two-domain wall process in a perfectly ordered array and monopole defects of opposite sign are found on opposite sides of the array early in the reversal process. The two-domain wall process is not observed to be the primary monopole defect formation mechanism in Co samples. This is due to quenched disorder in the lattice manifesting as a distribution of bar coercivities. A preliminary study shows that the use of magnetic injection pads can lead to reproducible monopole defect formation on the same lattice site. Our study shows that there is scope for controlled monopole defect formation and capture. Further work is needed to see the role of disorder and the extent of reproducibility further into the lattice.

Acknowledgments

We acknowledge funding from the EPSRC (EP/G004765/1) and the Leverhulme Trust (F/07058/AW). The authors would also like to acknowledge the use of the UK National Grid Service in carrying out this work.

References

- [1] Harris M J, Bramwell S T, McMorrow D F, Zeiske T and Godfrey K W 1997 Geometrical frustration in the ferromagnetic pyrochlore $\text{Ho}_2\text{Ti}_2\text{O}_7$ *Phys. Rev. Lett.* **79** 2554–57
- [2] Bramwell S T and Gingras M J P 2001 Spin ice state in frustrated magnetic pyrochlore materials *Science* **294** 1495–501
- [3] Castelnovo C, Moessner R and Sondhi S L 2008 Magnetic monopoles in spin ice *Nature* **451** 42–5
- [4] Bramwell S T, Giblin S R, Calder S, Aldus R, Prabhakaran D and Fennell T 2009 Measurement of the charge and current of magnetic monopoles in spin ice *Nature* **461** 956–9

- [5] Wang R F *et al* 2006 Artificial ‘spin ice’ in a geometrically frustrated lattice of nanoscale ferromagnetic islands *Nature* **439** 303–6
- [6] Ladak S, Read D E, Perkins G K, Cohen L F and Branford W R 2010 Direct observation of magnetic monopole defects in an artificial spin-ice system *Nat. Phys.* **6** 359–63
- [7] Qi Y, Brintlinger T and Cumings J 2008 Direct observation of the ice rule in an artificial kagome spin ice *Phys. Rev. B* **77** 094418
- [8] Donahue M J 1999 *OOMMF User’s Guide* (Gaithersburg, MD: NIST)
- [9] Park M H, Hong Y K, Choi B C, Donahue M J, Han H and Gee S H 2006 Vortex head-to-head domain walls and their formation in onion-state ring elements *Phys. Rev. B* **73** 094424
- [10] Garcia-Barriocanal J 2009 Tailoring disorder and dimensionality: strategies for improved solid oxide fuel cell electrolytes *Chem. Phys. Chem.* **10** 1003–11
- [11] Mellado P, Petrova O, Shen Y C and Tchernyshyov O 2010 Dynamics of magnetic charges in artificial spin ice *Phys. Rev. Lett.* **105** 187206
- [12] Ladak S, Read D, Tyliczszak T, Branford W R and Cohen L F 2011 Monopole defects and magnetic Coulomb blockade *New J. Phys.* **13** 023023
- [13] Petit D, Jausovec A V, Zeng H T, Lewis E, O’Brien L, Read D and Cowburn R P 2009 Mechanism for domain wall pinning and potential landscape modification by artificially patterned traps in ferromagnetic nanowires *Phys. Rev. B* **79** 214405